Micromagnetic simulation of switching events

Thomas Schrefl, Hermann Forster, Dieter Suess, Werner Scholz, Vassilios Tsiantos, and Josef Fidler

Institute of Applied and Technical Physics, Vienna University of Technology, A-1040 Vienna, Austria

Abstract. Magnetic switching of small particle, thin film elements and magnetic nano-wires becomes increasingly important in magnetic storage and magneto electronic devices. Micromagnetic switching events are studied using a hybrid finite element / boundary element method. The space discretization of the Gilbert equation leads to a system of ordinary differential equations. Its numerical integration provides the time evolution of the magnetization under the influence of an external field. Thermal fluctuations may be treated by a random field. The reversal mode drastically depends on the Gilbert damping constant. Decreasing the damping constant from $\alpha = 1$ to $\alpha \leq 0.1$ changes the reversal mode from uniform rotation to inhomogeneous switching. The decrease of the damping leads to the formation of vortices in circular nano-dots and to a nucleation process in columnar grains. Elongated Co particles revers by rotation if the length of the particle is smaller than 25 nm. Irreversible switching of longer particles occurs due to the formation of a nucleus of reversed magnetization and successive domain wall motion.

1 Introduction

The development of advanced magnetic materials such as magnetic sensors, recording heads, and magneto-mechanic devices requires a precise understanding of the magnetic behavior. These applications require a reproducible magnetic domain structure and a well-defined switching field of the individual magnetic elements. As the size of the magnetic components approaches the nanometer regime, detailed predictions of the magnetic properties becomes possible using micromagnetic simulations. Micromagnetism is a continuum theory for the treatment of magnetization processes in ferromagnetic materials. The micromagnetic equations describe the relation between the magnetic properties and the physical/chemical microstructure of the material. In addition to the hysteresis properties like remanence, coercive squareness, coercive field, the switching speed becomes increasingly important for magnetic data storage and magneto-electronic applications. With decreasing size of the magnetic structures, thermally activated reversal process become significant. Thermally induced reversal may influence the writing process as well as the long-term stability of written bits in magnetic recording.

The investigation of the switching behavior has been the subject of many recent experimental and theoretical work. Experimentally, in situ domain observation using Lorentz electron microscopy [1] and time resolved magnetic imaging [2] provides a detailed understanding domain formation and

reversal processes. The numerical solution of the Gilbert equation of motion provides the theoretical background for the switching process of ferromagnetic structures. The switching time considerably depends on the Gilbert damping constant α. Kikuchi [3] derived the critical value of α which minimizes the reversal time. Critical damping occurs for $\alpha = 1$ and $\alpha = 0.01$ for uniform rotation of the magnetization in a sphere and an ultra-thin film, respectively. Leineweber and Kronmller [4] investigated the reversal dynamics of small hard magnetic particles using a dynamic finite element method. They reported a waiting time after the application of an applied field, before the nucleation of reversed domains is initiated. Koch and coworkers [5] investigated the switching dynamics of micron-sized magnetic thin films experimentally and numerically. They observed switching times well below 500 ps. Albuquerque and co-workers [6] presented a finite difference method to effectively solve the Gilbert equation for thin film structured as used in current-tunnel junctions MRAM devices. A sequence of tailored field pulses causes a quasi-coherent switching in the subnanosecond regime, as short scale fluctuation are damped out quickly. Garcia-Palacíos and Lázaro [7] numerically solved the Langevin equation which describes magnetization processes at finite temperatures for a single magnetic moments. They reported important phenomena like crossing-back or multiple crossing of the energy barrier which are attributed to the gyromagnetic nature of the system. Zhang and Fredkin [8] used the finite element method to study thermally activated reversal in ellipsoidal particles large enough to show an inhomogeneous reversal process.

Finite element based micromagnetic codes effectively treat the microstructure of the system, including the shape of the magnet and the irregular grain structure [9]. The polyhedral shape of the magnetic particles leads to a non-uniform demagnetizing field which significantly influences the reversal process. Such as in finite element field calculation, micromagnetic finite element simulations introduce a magnetic scalar or magnetic vector potential to calculate the demagnetizing field. Fredkin and Koehler [10] proposed a hybrid finite element (FE) / boundary element (BE) method to treat the open boundary problem associated with calculation of the magnetic scalar potential. This method is accurate and allows to calculate the magnetostatic interaction between distinct magnetic elements without any mesh between the magnetic particles.

This work combines a hybrid finite element (FE) / boundary element (BE) method for the magnetostatic field calculation with the numerical interaction of the Gilbert equation of motion. Dynamic and thermal switching effects are investigated in circular nano-magnets, columnar grains, and magnetic nanowires. Section 2 of the paper describes the micromagnetic and numerical background of the simulation method. Section 3 presents numerical results on thermally activated switching of small particles and wires. The switching speed of magnetic wires results from the corresponding domain wall velocities

which are calculated in section 4. Section 5 treats the influence of the damping constant on the reversal processes in columnar grains and circular nano-dots.

2 Micromagnetic and numerical background

The theoretical treatment of thermally activated magnetization reversal requires to solve the Langevin equation numerically. The Langevin equation follows from the Gilbert equation of motion by adding a random thermal fluctuation field to the effective magnetic field. The deterministic Gilbert equation [11] is believed to describe the physical path of the magnetization towards equilibrium, taking into account gyromagnetic precession and damping. In real systems, thermal fluctuations changes the deterministic motion of the magnetization into a random walk. A theoretical description must treat magnetization reversal as stochastic process. The magnetic properties like the coercive field and the switching time follow from averages over many numerical realizations of the reversal process.

2.1 Langevin micromagnetics

The Langevin equation [12]

$$\frac{\partial \mathbf{J}}{\partial t} = -|\gamma| \mathbf{J} \times (\mathbf{H}_{\mathrm{eff}} + \mathbf{H}_{\mathrm{th}}) + \frac{\alpha}{J_{\mathrm{s}}} \mathbf{J} \times \frac{\partial \mathbf{J}}{\partial t} \tag{1}$$

describes the random motion of the magnetic polarization vector $\mathbf{J} = (J_1, J_2, J_3) = \mu_0 \mathbf{M}$ at finite temperatures. The first term on the right hand side of equation (1) accounts for the gyromagnetic precession, the second term arises from viscous damping. γ is the gyromagnetic ratio of the free electron spin $\gamma = 2.21 \times 10^5$ m/(As); α is the Gilbert damping constant. The critical value of α which minimizes the relaxation time was found to $\alpha = 1$ at zero temperature [3] and thermally activated reversal [13]. The effective field, $\mathbf{H}_{\mathrm{eff}} = -\delta E_{\mathrm{t}} / \delta \mathbf{J}$, is the variational derivative of the total magnetic Gibbs free energy

$$E_{\mathrm{t}} = \int_{\Omega_{\mathrm{int}}} dV \left\{ \frac{A}{J_{\mathrm{s}}^2} \sum_{i=1}^{3} (\nabla J_i)^2 - \frac{K_{\mathrm{u}}}{J_{\mathrm{s}}^2} (\mathbf{J} \cdot \mathbf{u})^2 - \frac{1}{2} \mathbf{J} \cdot \mathbf{H}_{\mathrm{d}} - \mathbf{J} \cdot \mathbf{H}_{\mathrm{ext}} \right\}. \tag{2}$$

E_{t} is the sum of the exchange energy density, the magneto-crystalline anisotropy energy density, the magnetostatic energy density, and the Zeeman energy density. A is the exchange constant, $J_{\mathrm{s}} = |\mathbf{J}|$ is spontaneous magnetic polarization, K_{u} is the uniaxial anisotropy constant, and $\mathbf{u}$ is the anisotropy direction. $\mathbf{H}_{\mathrm{ext}}$ is the external field. The demagnetizing field $\mathbf{H}_{\mathrm{d}}$ follows from the magnetic scalar potential $\mathbf{H}_{\mathrm{d}} = -\nabla U$ which satisfies the Poisson equation inside the magnetic particles and Laplace equation outside the magnets.

In order to treat thermally activated processes a stochastic, thermal field, $\mathbf{H}_{\mathrm{th}}$, is added to the effective field, $\mathbf{H}_{\mathrm{eff}}$. The thermal field is assumed to be a Gaussian random process with the following statistical properties:

$$\langle H_{\mathrm{th},i}\left(\mathbf{r},t\right)\rangle = 0, \tag{3}$$

$$\langle H_{\mathrm{th},i}\left(\mathbf{r},t\right) H_{\mathrm{th},j}\left(\mathbf{r}',t'\right)\rangle = D\delta_{ij}\delta\left(\mathbf{r}-\mathbf{r}'\right)\delta\left(t-t'\right). \tag{4}$$

The average of the thermal field, taken over different realizations, vanishes in each direction i in space. The thermal field is uncorrelated in time and space. The strength of the thermal fluctuations follow from the fluctuation-dissipation theorem [14]:

$$D = \frac{2\alpha k_{\mathrm{B}}T}{\gamma J_{\mathrm{s}}}. \tag{5}$$

2.2 Space and time discretization

The Cartesian components of the magnetic polarization vector, $\mathbf{J}$, and the magnetic scalar potential, U, are interpolated with piecewise linear functions on a tetrahedral finite element mesh. A hybrid finite element / boundary element method is used to solve the magnetostatic boundary value problem. The effective field at the node k of the irregular finite element mesh may be approximated using a box scheme:

$$\mathbf{H}_{\mathrm{eff}}^{(l)} \approx -\frac{1}{V^{(l)}}\frac{\partial E_{\mathrm{t}}\left(\ldots,\mathbf{J}^{(l-1)},\mathbf{J}^{(l)},\mathbf{J}^{(l+1)},\ldots\right)}{\partial\mathbf{J}^{(l)}} \tag{6}$$

where $V^{(l)}$ is the volume associated with the node l. The following conditions hold for the box volumes

$$\sum_l V^{(l)} = \int_{\Omega_{\mathrm{int}}} dV \quad \text{and} \quad V^{(l)} \cap V^{(m)} = 0 \quad \text{for } l \neq m. \tag{7}$$

The Langevin equation (1) is solved using the method of Heun. It reduces to three stochastic differential equations for each node of the finite element mesh, using the box scheme (6) to approximate the effective field. For $T = 0$ the Langevin equation reduces to a system of ordinary differential equation which is solved using backward difference formulas or higher order Adams methods, depending on the stiffness of the equations [15].

3 Thermally activated switching

The basic structural units of magnetic recording media are particles or grains in the nanometer range. Data is stored in small regions consisting of several grains or particles which have their magnetization oriented in two allowed

directions. With increasing recording density the grain size as well as the number of grains or particles forming a bit becomes smaller. With decreasing size of the elementary storage volumes, thermally activated magnetization reversal becomes an important issue in magnetic recording [16]. Thermal activation governs the time dependence of the magnetization. Therefore, thermal effects are relevant to the high speed switching of the magnetization in the write process and to the long term thermal stability of the written bit. The irreversilbe switchig of the particle occurs either by the rotation of the magnetization or by the expansion of a nucleus of reverse magnetization. Both processes are associated with activation energy and may be described using the Arrhenius-Néel model. At finite temperatures, random magnetic field fluctuations help to overcome the reversal barrier [17,18]. The stochastic fluctuation field arises from the interplay of the lattice vibrations and the magnetization. The probability of irrversible switching is given by the probability per unit time of crossing the energy barrier

$$p = f_0 \exp(-E/k_\mathrm{B}T), \tag{8}$$

where f_0 is a thermal attempt frequency for barrier crossing, k_B denotes the Boltzmann factor, and T is the temperatur. The reciprocal of the switching probability is the relaxation time

$$\tau = f_0^{-1} \exp(E/k_\mathrm{B}T). \tag{9}$$

The attempt frequency f_0 depends on material parameters, like anisotropy, particle shape, and damping [19], The value which ranges from $f_0 = 10^9$ Hz to $f_0 = 10^{12}$ Hz sets the time scale for thermally assisted magnetization reversal $\tau_0 = f_0^1 \approx 1$ ns.

The activation energy and the attempt frequency can be estimated for coherent rotation of the magnetizatio in single domain particles [18] and the nucleation of reversed domains in thin ferromagnetic wires [19]. The intrinsic magnetic properties of Co ($J_\mathrm{s} = 1.76$ T, $A = 1.3 \times 10^{-11}$, $K_\mathrm{u} = 6.8 \times 10^5$ J/m^3) and a Gilbert damping constant $\alpha = 1$ were assumed for the calculations. The particles have a diameter $d = 2$ nm and an aspect ratio of 2:1, 4:1, and 16:1, respectively.

3.1 Thermally activated reversal of ellipsoidal particles

The extension of the ellipsoid is comparable with the exchange length, l_ex. Thus it is expected to reverse by coherent rotation. According to the Stoner-Wohlfarth theory the field dependence of the activation energy, $E(H)$, is [20]:

$$E(H) = KV \left(1 - \frac{H}{H_\mathrm{K}}\right)^2, \tag{10}$$

$$K = K_{\mathrm{u}} + \frac{J_{\mathrm{s}}^2}{2\mu_0}\left(N_\perp - N_\parallel\right), \tag{11}$$

$$H_{\mathrm{K}} = \frac{2K}{J_{\mathrm{s}}}. \tag{12}$$

K is the effective anisotropy constant taking into account the shape of the particle; V is the particle volume; $N_\parallel$ and $N_\perp$ are the demagnetizing factors parallel and normal to the symmetry axis. A fit of the calculated relaxation time τ using equation (2) provides the energy barrier from numerical experiments. Fig. 1 shows that $\ln\tau$ versus $1/\left(k_{\mathrm{B}}T\right)$ forms a straight line in the investigated field and temperature range.

Fig. 1. Relaxation time as a function of $KV/\left(k_{\mathrm{B}}T\right)$ for different applied fields. The inset gives the finite element model of the ellipsoidal particle.

3.2 Thermally induced nucleation in magnetic nano wires

The cylindrical particle with an aspect ratio of 4:1 reverses by uniform rotation. Again the relaxation time as a function of the inverse temperature forms a straight line in a semi-logarithmic plot.

The formation of a nucleus of reverse magnetization at the end starts the reversal process in the nanowire with aspect ratio 16:1. Using an analytical model, Braun [21] estimated the energy barrier for the nucleation in a nanowire

$$E(H) = (8/3)r^2\pi\sqrt{AK}\left(1 - \frac{H}{H_{\mathrm{K}}}\right)^{3/2}, \tag{13}$$

where r is the radius of the wire. Fig. 2 gives the energy barriers, $E(H)$, as a function of the field for the ellipsoid and the nanowire with the aspect ratio 16:1. For the ellipsoid, the numerical values for the activation energy

agree perfectly with the analytical results given by equation (10). For the nanowire, the energy barriers according to equation (13) exceed the numerical results by about a factor of 2 to 3. This may be attributed to inhomogeneous magnetic states across the wire, which are neglected in the analytical model. These magnetic inhomogeneities arise from thermal fluctuations and the highly nonuniform demagnetizing field near edge at the ends of the wire.

An effective activation volume can be derived under the assumption that the activation energy corresponds to the energy of the nucleus of reverse magnetization

$$E(H) = -vJ_{\mathrm{s}}H. \tag{14}$$

Then the activation volume, v, can be derived from the slope of $E(H)$

$$v = -\frac{1}{J_{\mathrm{s}}}\frac{\partial E}{\partial J}. \tag{15}$$

Fig. 3 clearly shows that the activation energy for the wire depends linearly on the applied field within the investigated field range. This behavior indicates that magnetization reversal occurs by the formation of a nucleus of reverse magnetization [20]. The analysis of the calculated magnetization configurations as a function of time confirms a nucleation mechanism. The magnetization starts to reverse within a finite volume at one end of the wire. Once a reversed domain has formed, it expands over along the entire wire. The calculated activation volume, $v = (2.1\ \mathrm{nm})^3$, was found to be independent of the length of the nanowire. Li and co-worker [22] obtained a similar result from magnetic measurements on α-Fe nanowires.

Fig. 2. Activation energy as a function of the applied field. The open symbols give the numerical values. The dashed lines give the analytical results according to equation (10) and (13). The dotted line is linear fit of the numerical values for the nanowire.

4 Domain wall motion in magnetic nano-wires

The total reversal time of a magnetic wire is the sum of the relaxation time to create a nucleus of reverse magnetization and the time required for the expansion of the reversed domain. The latter is associated with the domain wall velocity. The domain wall velocity was calculated as a function of the applied field for a Co-nanowire with a diameter of 40 nm. The Gilbert damping constant was $\alpha = 0.1$. The expansion of a reversed domain under the influence of an applied field was investigated for Co-wires with a length of 600 nm. The average magnetization parallel to the long axis was found to decrease linearly with time as long as the domain wall was far away from the ends. The slope of the curve increases with increasing field strength. Fig. 3 shows the calculated wall velocity as a function of the applied field.

Fig. 3. Domain wall velocity calculated for a Co-nanowire with a diameter of 40 nm and a Gilbert damping constant $\alpha = 0.1$. The inset maps the magnetization component parallel to the field at the surface of the wire.

An adaptive mesh refinement scheme [23] was used for the simulations. The finite elements are subdivided near the center of the wall, whereas a coarse grid is used in regions where the magnetization is nearly uniform. During the simulations, the mesh is adjusted to the current wall position. The adaptive mesh scheme keeps the number of finite elements low while resolve the micromagnetic details of the wall structure.

Fig. 4 compares the time evolution of the magnetization for a coarse uniform grid, a fine uniform grid, and the adaptive grid. The results clearly show that a fine enough grid is required to obtain the linear dependence of the magnetization as a function of time. However, instead of a fine uniform grid, the adaptive mesh method can be used. It provides nearly similar results for the wall velocities and drastically decreases the CPU time.

Fig. 4. Adaptive meshing and CPU time. The solid lines give the magnetization parallel to the long axis as a function of time for a coarse uniform grid, a fine uniform grid, and an adaptive grid. The dashed curves compare the CPU time (Athlon 900 Mhz) required on the uniform grid and on the adaptive grid.

5 Influence of the damping constant

5.1 Columnar grains

In recent years there has been a renewed interest in perpendicular recording since an improvement of the areal density in longitudinal recording is getting increasingly difficult. The main advantage of perpendicular recording is that the areal density can be increased without reducing the volume of the magnetic bit. A large volume of the magnetic domain can be realized with an increased column length (film thickness). For coherent rotation a higher grain volume leads to a higher energy barrier and hence to an improved thermal stability. However, if the column length becomes to large the reversal mode might change from uniform rotation to nucleation. The latter process has an energy barrier which is independent of the column length [24]. In the following the maximum exchange energy during reversal was used to distinguish between the two reversal modes.

Fig. 5 compares the exchange energy as a function of the column length for high and low damping. Vanishing exchange energy indicates uniform rotation. Clearly, a small damping constants induces the nucleation of a reversed domain for small particles even for a small column length.

5.2 Circular nanomagnets

Micromagnetic simulations of magnetization reversal in circular nano-magnets show that the reversal process strongly depends on the thickness of the elements [25]. With increasing thickness demagnetizing field becomes important leading to partial flux-closure structures during reversal, if the diameter of

Fig. 5. Maximum exchange energy during reversal as a function of the column length. The inset gives the shape of the irregular grain.

the nano-dot is greater of equal 110 nm. For the very same reason vortices form during the reversal process for a thickness of 15 nm and a diameter greater or equal 165 nm.

Fig. 6. Time evolution of the magnetization component parallel to the applied field during the reversal of a nano-dot with a thickness of 15 nm and a diameter of 165 nm for small and large damping. The inset shows the finite element model.

Fig. 6 compares the time evolution of the magnetization for different damping constant. For $\alpha = 1$ the nano-dot start to switch only after a waiting time of about 3 ns. For $\alpha = 0.01$ the waiting time reduces to about 0.5 ns. Fig. 7 shows that the reversal process changes if the damping constant is decreased. For $\alpha = 1$ inhomogeneous rotation occurs. For $\alpha = 0.01$ vortexes are formed during reversal. Whereas in simulations with $\alpha = 1$ only one vortex occurs (provided the samples have an large enough diameter and thickness), for $\alpha = 0.01$ two vortices are formed at the beginning (A in Figs. 6 and 7).

Fig. 7. Vortex formation and vortex movement during the reversal of a nano-dot with a thickness of 15 nm and a diameter of 165 nm for small and large damping.

These two vortexes combine to one vortex after 1 ns. As a consequence the magnetic polarization increases until one big vortex is formed (B in Figs. 6 and 7).

6 Acknowledgements

The authors thank Denise Hinzke and Ulrich Nowak for helpful discussions. This work was supported by the Austrian Science Fund (Y132-PHY, 13260 TEC) and the European COST P3 action.

References

1. K. J. Kirk, J. N. Chapman and C. D. W. Wilkinson: Switching fields and magnetostatic interactions of thin film magnetic nanoelements, Appl. Phys. Lett. **71**, 539–541 (1997)
2. C. H. Back, J. Heidmann, J. McCord: Time resolved Kerr microscopy: Magnetization dynamics in thin film write heads,IEEE Trans. Magn. **35**, 637–642(1999)
3. R. Kikuchi: On the minimum of magnetization reversal time, J. Appl. Phys. **27**, 1352–1357 (1956)
4. T. Leineweber, H. Kronmüller: Dynamics of magnetisation states, J. Magn. Magn. Mater. **192**, 575–590 (1999)
5. R. H. Koch et al.: Magnetization reversal in micron-sized magnetic thin films, Phys. Rev. Lett. **81**, 4512–4515 (1998)
6. G. Albuquerque, J. Miltat, A. Thiaville: Coherent spin structures dynamics: numerics and application th high density magnetic random access memories (MRAMs), in , 16th IMACS World Congress On Scientific Computation, Applied Mathematics and Simulation, Lausanne, Switzerland, 2000, M. Deville, R. Owens (Eds.)
7. J. L. García-Palacios, F. J. Lázaro: Langevin-dynamics study of the dynamical properties of small magnetic particles, Phys. Rev. B **58** 14937–14958 (1998)
8. K. Zhang, D. R. Fredkin: Stochastic dynamic micromagnetic study of fine particles, J. Appl. Phys. **85** 5208–5210 (1999)

9. T. Schrefl, J. Fidler: Modelling of Exchange-Spring Permanent Magnets, J. Magn. Magn. Mater. **177** 970–975 (1998)
10. D. R. Fredkin, T. R. Koehler: Hybrid method for computing demagnetizing fields, IEEE Trans. Magn. **26** 415–417 (1990)
11. T. L. Gilbert: A Lagrangian formulation of gyromagnetic equation of the magnetization field, Phys. Rev. **100**, 1243 (1955)
12. W.F. Brown, Jr.:, *Micromagnetics*, (Wiley, New York, 1963)
13. D. Hinzke, U. Nowak: Magnetization switching in nanowires: Monte Carlo study with fast Fourier transformation for dipolar fields, J. Magn. Magn. Mater., to appear.
14. N.G. van Kampen: *Stochastic processes in physics and chemistry*, (Norh-Holland, Amsterdam, 1992)
15. A. C. Hindmarsh, L. R. Petzold: Algorithms and software for ordinary differential equations: part II: higher order methods and software packages, Computers in Physics **9**, 148–155 (1995)
16. D. Weller, A. Moser: Thermal effect limits in ultrahigh-density magnetic recording, IEEE Trans. Magn. **35**, 4423–4439 (1999)
17. L. Néel: Théorie du trainage magnétique, Ann. Geophys. **5**, 99–136 (1949)
18. W. F. Brown, Jr.: Thermal fluctuations of a single-domain particle, Phys. Rev. **130**, 1677–1686 (1963)
19. H.-B. Braun: Kramers's rate theory, broken symmetries, and magnetization reversal (invited), J. Appl. Phys. **76** 6310–6315 (1994)
20. R. Street, D.C. Crew: Fluctuation aftereffects in magnetic materials, IEEE Trans. Magn. **35** 4407–4413 (1999)
21. H.-J. Braun, Nucleation in ferromagnetic nanowires—magnetostatics and topology, J. Appl. Phys. **85** 6172–6174 (1999)
22. F.L. Li, R.M. Metzger, W.D. Doyle: Influence of particle size on the magnetic viscosity and activation volume of α-Fe nanowires in alumite films, IEEE Trans. Magn. **33** 4423–4439 (1997)
23. W. Scholz, T. Schrefl and J. Fidler: Mesh refinement in FE-micromagnetics for multi-domain Nd2Fe14B particles, J. Magn. Magn. Mater. **196–197** 933–934 (1999)
24. D. Suess, T. Schrefl and J. Fidler: Reversal modes, thermal stability, and exchange length in perpendicular recording media, IEEE Trans Magn. (in press)
25. D. Suess, T. Schrefl, J. Fidler and V. Tsiantos: Reversal dynamics of interacting circular nanomagnets, IEEE Trans Magn. (in press)

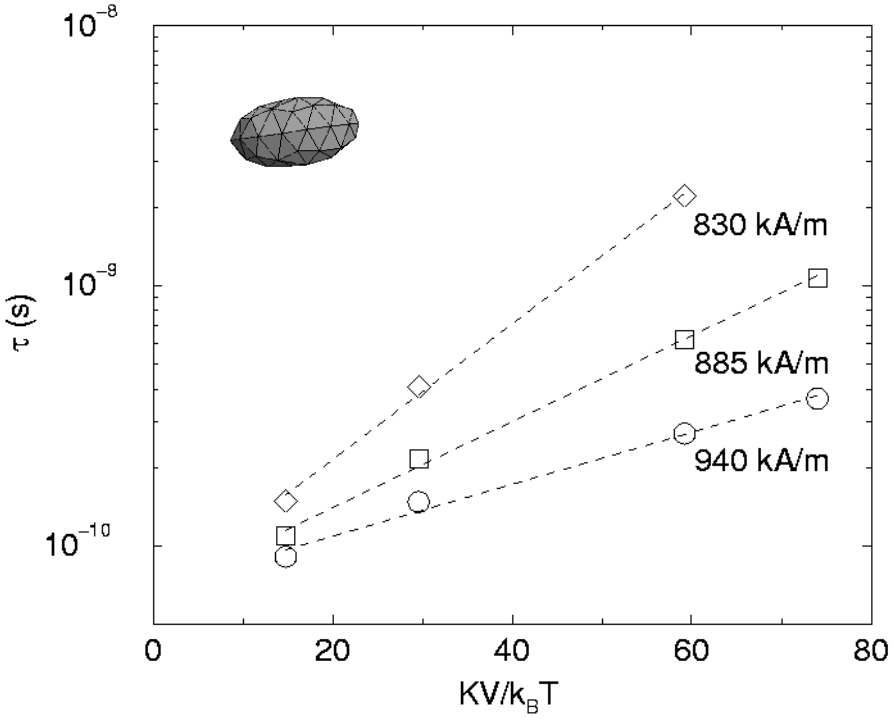

Fig. 1. Relaxation time as a function of *KV*/*kT* for different applied fields. The inset gives the finite element model.

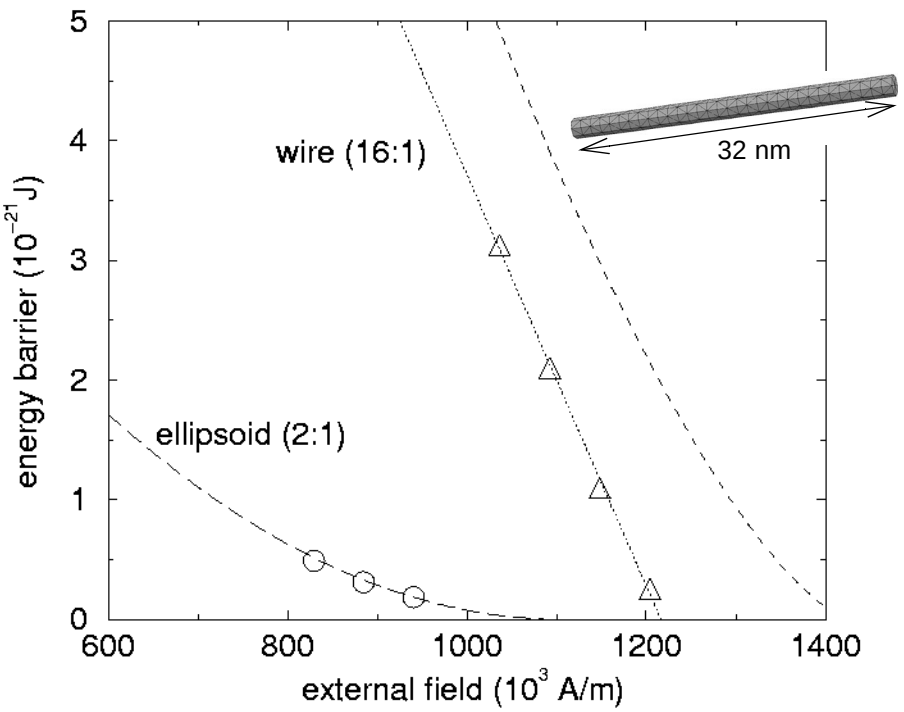

Fig. 2. Activation energy as a function of the applied field. The open symbols give the numerical values. The dashed lines give the analytical results according to equation (10) and (13). The dotted line is linear fit of the numerical values for the nanowire.

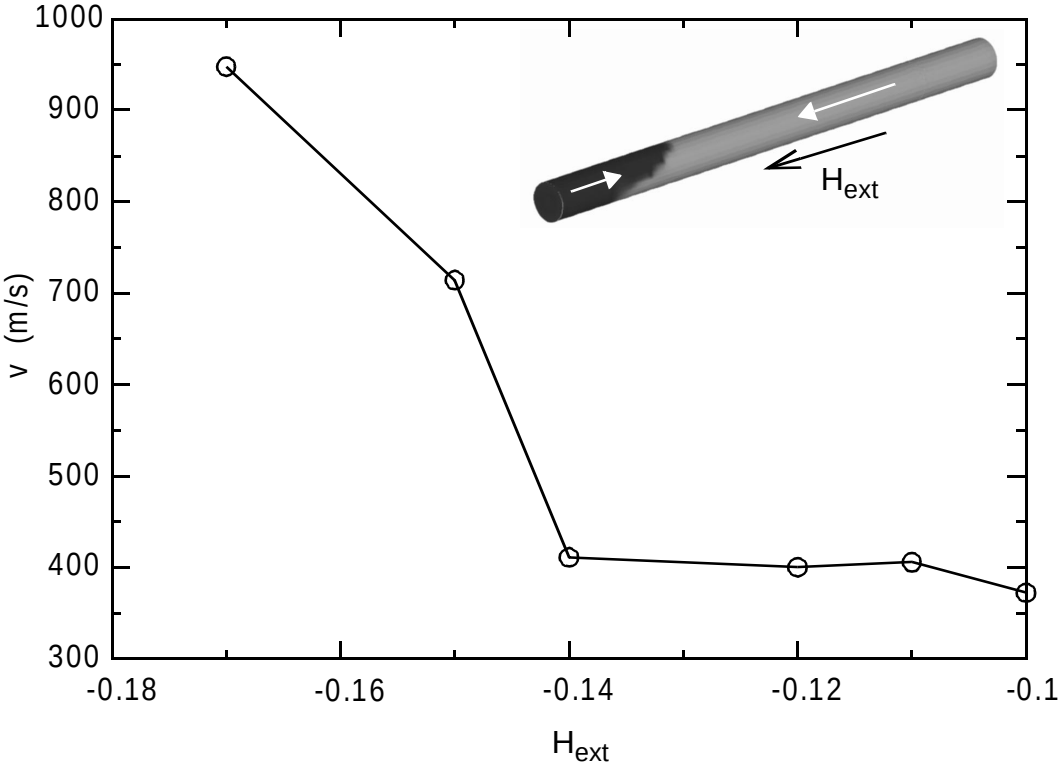

Fig. 3. Domain wall velocity calculated for a Co-nanowire with a diameter of 40 nm and a Gilbert damping constant $\alpha = 0.1$. The inset maps the magnetization component parallel to the field at the surface of the wire.

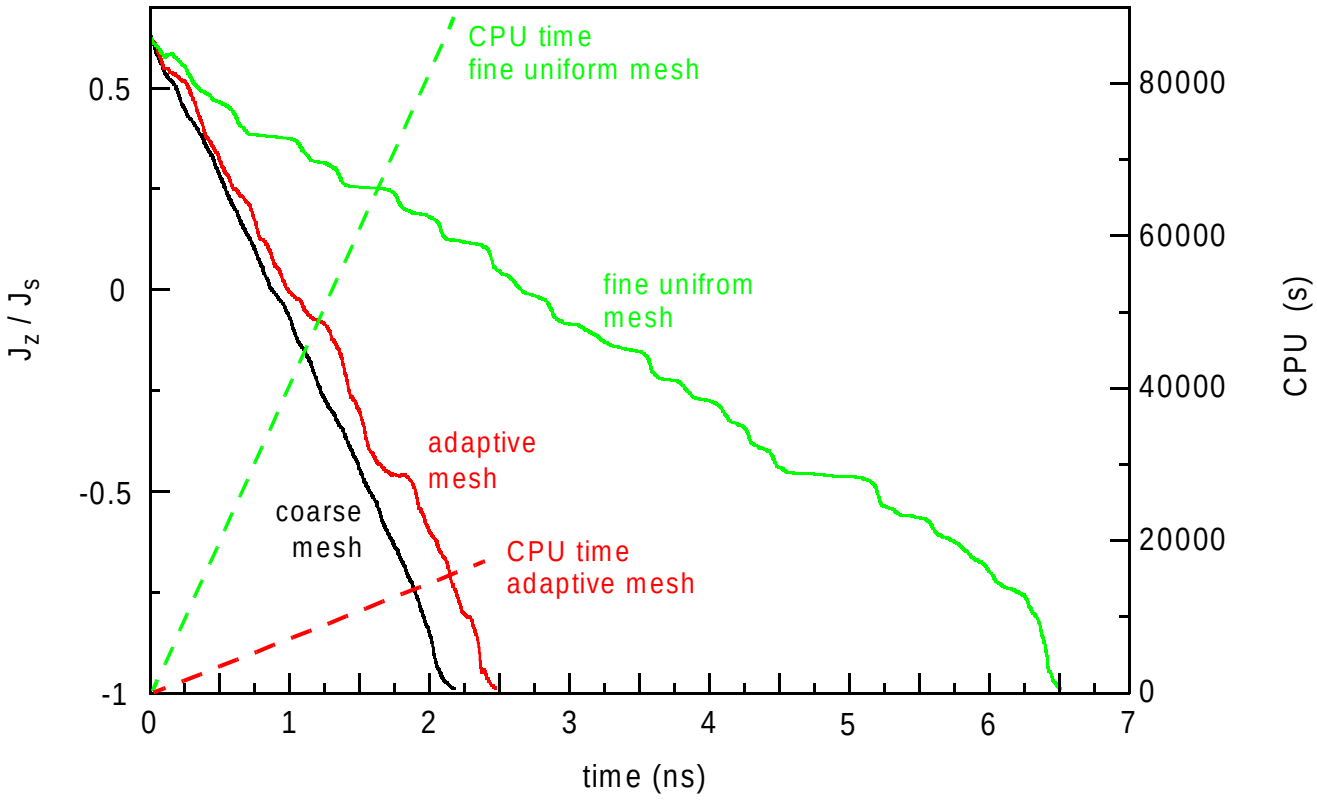

Fi.g 4. Adaptive meshing and CPU time. The solid lines give the magnetization parallel to the long axis as a function of time for a coarse uniform grid, a fine uniform grid, and an adaptive grid. The dashed curves compare the CPU time (Athlon 900 Mhz) required on the uniform grid and on the adaptive grid.

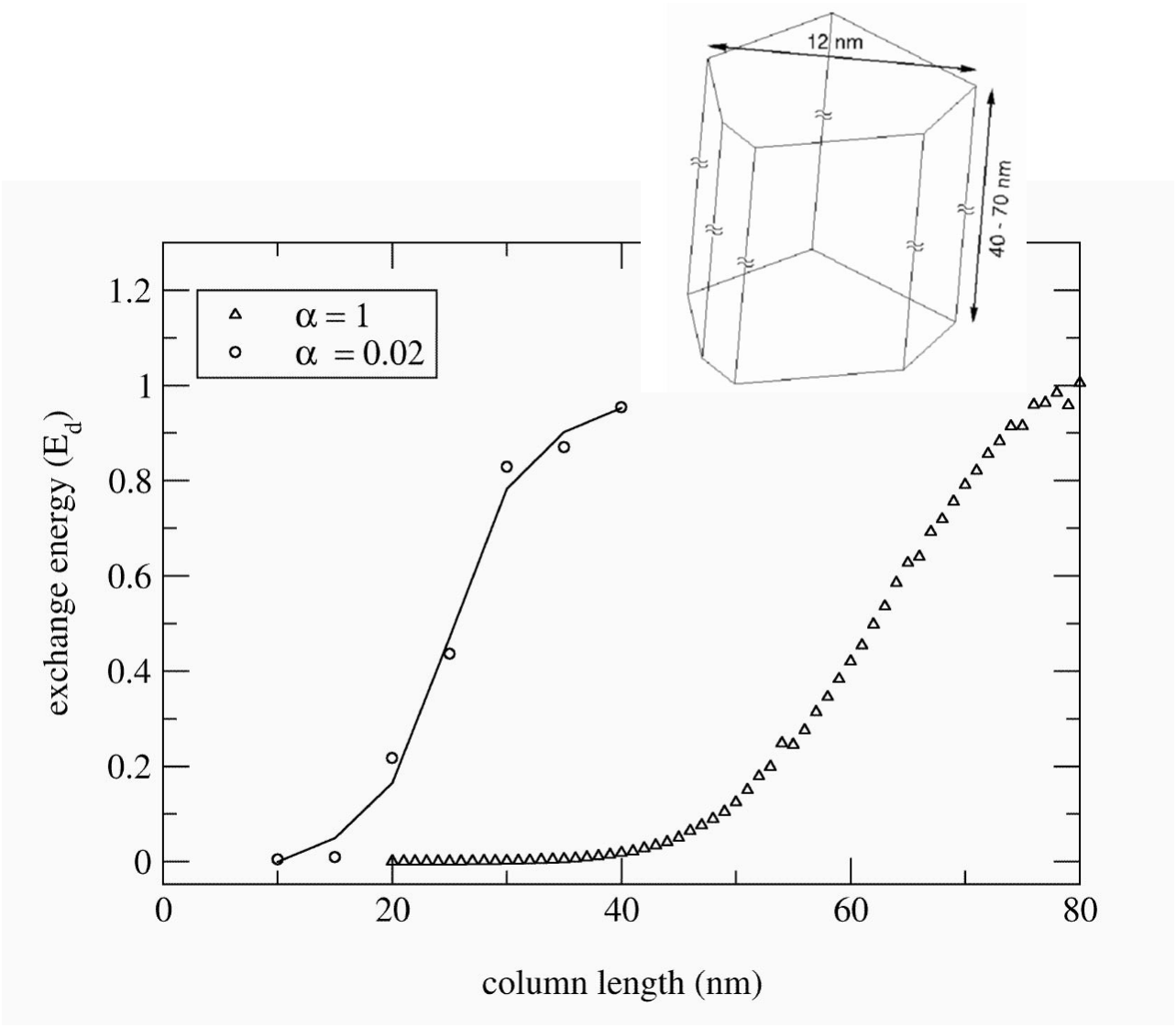

Fig. 5. Maximum exchange energy during reversal as a function of the column length. The inset gives the shape of the irregular grain.

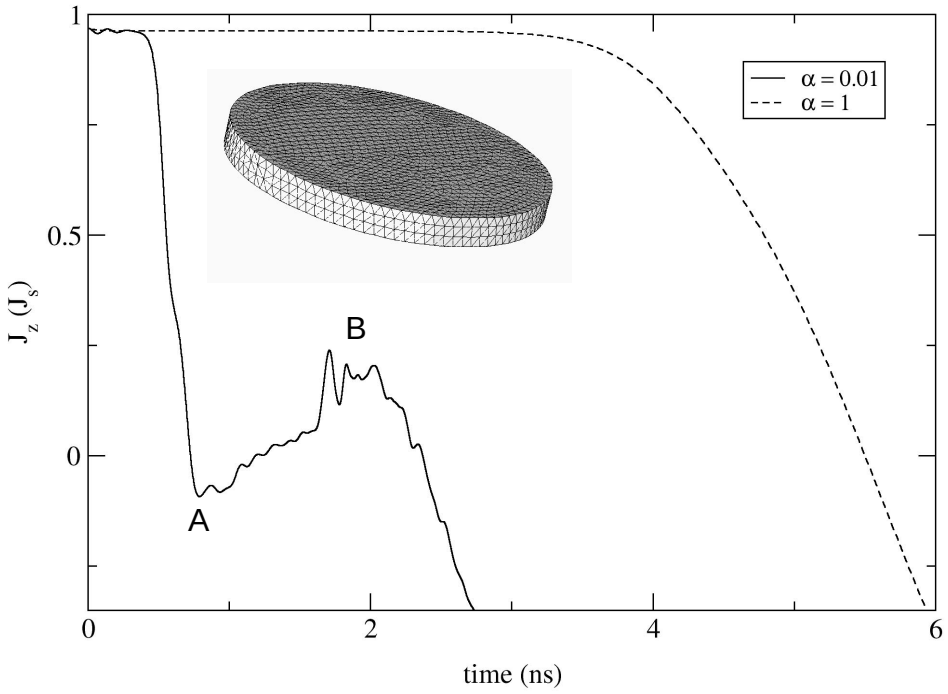

Fig. 6. Time evolution of the magnetization component parallel to the applied field during the reversal of a nano-dot with a thickness of 15 nm and a diameter of 165 nm for small and large damping. The inset shows the finite element model.

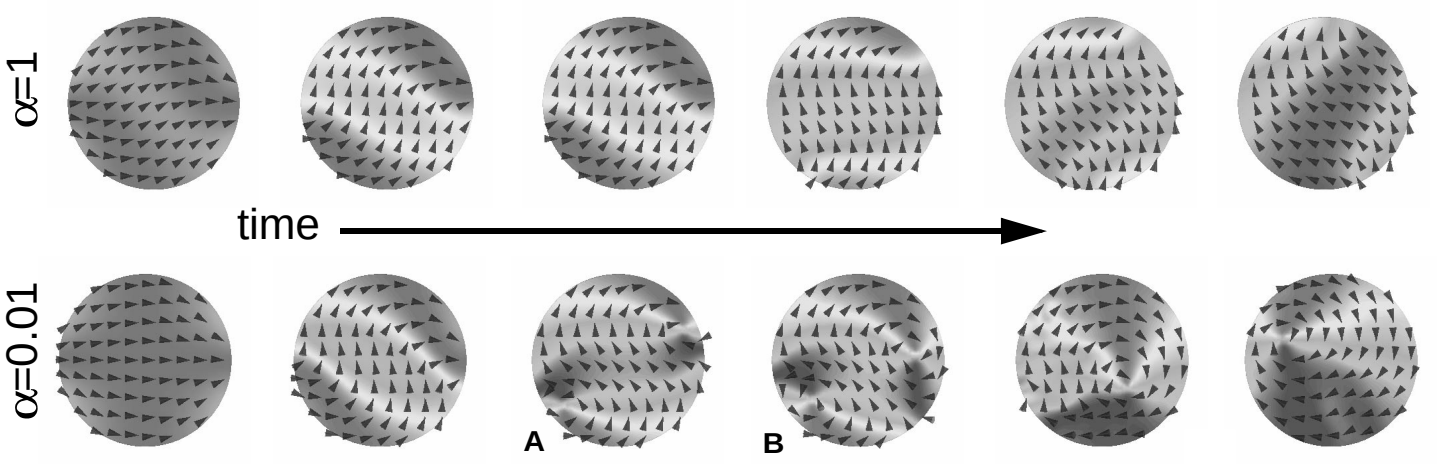

Fig. 7. Vortex formation and vortex movement during the reversal of a nano-dot with a thickness of 15 nm and a diameter of 165 nm for small and large damping.